One- and Two-Dimensional Solid-State ^{13}C NMR Analyses of the Solid Structure and Molecular Motion of Poly(ϵ-caprolactone) Isothermally Crystallized from the Melt

Hironori Kaji and Fumitaka Horii*

Institute for Chemical Research, Kyoto University, Uji, Kyoto 611, Japan

Received February 5, 1997; Revised Manuscript Received May 13, 1997[⊗]

ABSTRACT: The crystalline−noncrystalline structure and molecular motion of poly(ϵ-caprolactone) (PCL) isothermally crystallized from the melt have been investigated by one- and two-dimensional solid-state ^{13}C NMR spectroscopy. The ^{13}C spin−lattice relaxation time (T_{1C}) analysis reveals that the PCL sample contains three components with different T_{1C} values, which are assignable to the crystalline, mobile crystalline, and noncrystalline components. By the ^{13}C spin−spin relaxation time (T_{2C}) analysis, it is found that the noncrystalline component can be further resolved into the crystalline−amorphous interfacial, and amorphous components. The mass fractions of the crystalline, interfacial, and amorphous components are finally determined to be 0.42, 0.30, and 0.28, respectively. In the crystalline region, different molecular mobilities along the methylene sequence are suggested through the difference in T_{1C} value for the constituting carbons. More detailed molecular motion in the crystalline region has been characterized by the analysis of the ^{13}C chemical shift anisotropy (CSA) in terms of the two-site exchange model. ^{13}C CSA spectra of the individual carbons are successfully recorded by using the two-dimensional switching angle sample spinning technique. The CSA spectrum of the carbonyl carbon exhibit that the carbonyl carbon is almost in the rigid state or undergoes the jump motion around the molecular chain axis with a jump angle less than 30°. In contrast, methylene carbons exhibit almost axially symmetric CSA spectra, suggesting the rapid jump motions around the molecular chain axis with a jump angle of 60−90°. Further narrowed CSA spectra, which are still axially symmetric, are observed for the methylene carbons not directly attached to the ester group, suggesting the existence of additional enhanced jump motion around the C−C bonds. Such enhanced molecular motions of the methylene sequence may be due to the distorted nonplanar zigzag chain conformation of PCL in the crystalline region.

Introduction

Poly(ϵ-caprolactone) (PCL) is of great interest as a biodegradable polymer. This polymer is also nontoxic and has potential as a polymer device for the controlled release of drugs.[1] PCL is a crystalline polymer, and the crystal structure has been determined by X-ray diffraction[2,3] and electron diffraction[4] measurements. However, the crystalline−noncrystalline structure and the molecular motion of PCL have not been well characterized as yet.

Solid-state NMR is a powerful technique for the elucidation of the detailed structure of solid polymers.[5] To date, we have clarified the crystalline−noncrystalline structure for different crystalline polymers, such as polyolefins,[6−9] polyether,[10] polyester,[11] poly(vinyl alcohol),[12,13] polyurethane,[14] and cellulose.[15,16] Precise analyses of ^{13}C resonance line shapes, spin−lattice (T_{1C}), and spin−spin (T_{2C}) relaxation behaviors and ^{1}H spin diffusion have revealed that some of these polymers are composed of the crystalline, crystalline−amorphous interfacial, and amorphous regions in the solid state.

Solid-state NMR also gives us important information about the molecular motion of polymers.[17,18] The wide frequency range of motion is covered by the solid-state NMR spectroscopy: rapid motion with the frequency of 10^8−10^{12} Hz can be characterized by the analysis of spin relaxation parameters, such as T_1 and T_2. The information about the 10^2−10^8 Hz motion can be obtained by the line shape analyses of chemical shift anisotropy (CSA) spectra, wide-line ^{2}H spectra, and ^{1}H−^{1}H or ^{13}C−^{1}H dipolar spectra. Their multidimensional exchange spectra also give us the detailed information about the ultraslow motion with 10^{-1}−10^{1} Hz.

In this paper, solid-state ^{13}C NMR analyses are carried out on the PCL sample isothermally crystallized from the melt. The crystalline−noncrystalline structure is characterized by analyzing the gated decoupled/MAS spectrum and T_{1C} and T_{2C} relaxation processes. The molecular motion, particularly in the crystalline region, is also investigated by analyzing T_{1C}, CSA line shapes, and two-dimensional ^{13}C CSA exchange spectra.

Experimental Section

Sample. PCL with M_n = 80 000, which was provided by Unitika Ltd., was melted at 100 °C for 1 h and then isothermally crystallized at 50 °C for 4 days in an argon atmosphere. The sample thus obtained was cut into pieces with the dimension about 1 × 1 × 1 mm. PCL fibers with a draw ratio of 5, which were also provided by Unitika Ltd., were used for the assignment of the principal axes of CSA for this material.

Solid-State ^{13}C NMR Measurements. Solid-state ^{13}C NMR measurements were conducted on a JEOL JNM-GSX200 spectrometer operating under a static magnetic field of 4.7 T. The ^{1}H and ^{13}C field strengths $\gamma B_1/2\pi$ were 62.5 kHz. The contact time for the CP process was 2.0 ms, and the rate of sample spinning was set to 3 kHz throughout this work. ^{13}C chemical shifts were expressed as values relative to tetramethylsilane (Me_4Si) by using the CH_3 line at 17.36 ppm for hexamethylbenzene crystals as an external reference. The sample temperature was calibrated using the temperature dependence[19] of relative chemical shifts of CH_2 and OH protons of ethylene glycol in a glass ampule, which was packed with KBr in a MAS rotor.[11] All the measurements were carried out at room temperature, and the calibrated temperature was 41 °C at the spinning rate of 3 kHz.

T_{1C} values longer than 10 s were measured by the CPT1 pulse sequence,[20] while the shorter values were determined by the saturation-recovery pulse sequence without CP.[6,10] T_{2C} relaxation decays were measured by the spin echo pulse sequence modified for solid-state measurements.[6,10] Here, ^{1}H dipolar decoupling was not used during the T_{2C} decay. The

[⊗] Abstract published in *Advance ACS Abstracts,* September 1, 1997.

S0024-9297(97)00167-8 CCC: $14.00

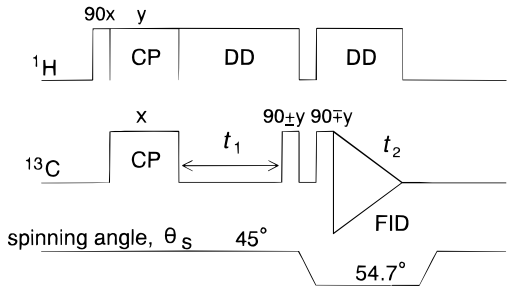

Figure 1. Phase sensitive 2D SASS pulse sequence for the measurement of individual CSA spectra. The spinning angle is set to be 45° and the magic angle during the evolution period t_1 and the detection period t_2, respectively. The short T_{1C} component is greatly reduced in intensity by storing the magnetization to the $+z$ and $-z$ directions alternatively during the angle switching period.

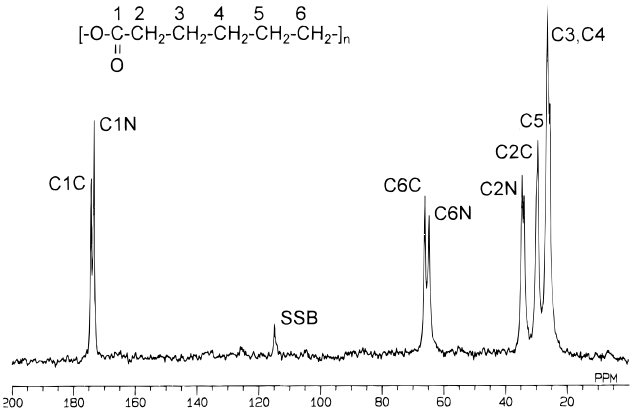

Figure 2. Gated decoupled/MAS ^{13}C NMR spectrum of solid PCL.

fully relaxed, gated decoupled ^{13}C NMR spectrum was obtained by the 45 single pulse with the waiting time $\tau_1 = 1200$ s after the acquisition of an FID, which was longer than 3 times the longest T_{1C} value for the sample.

CSA powder patterns were measured by the two-dimensional switching angle sample spinning (2D SASS) method[21−23] with the use of a Doty Scientific DAS probe in order to separate the CSA for different carbons. The phase sensitive 2D SASS pulse sequence used in this work is shown in Figure 1. The spinning angles were switched between 45° and the magic angle within 50 ms. The assignments of the principal axes for CSA were carried out by the measurements of CP/dipolar decoupled ^{13}C NMR spectra for the uniaxially oriented PCL fibers. The orientation axis was set to be either parallel or perpendicular to the static magnetic field B_0 in the measurements.

Two-dimensional ^{13}C CSA exchange spectra were measured by off magic angle spinning with the angle of 45°. Mixing times were set to be 0.1, 1, and 3 s.

Results and Discussion

Gated Decoupled/MAS ^{13}C NMR Spectrum. Figure 2 shows the fully relaxed, gated decoupled/MAS ^{13}C NMR spectrum of PCL, which quantitatively reflects all the components included in the sample. The assignment of each resonance line has been made on the basis of the results for the solution-state spectrum.[24] The resonance lines of C1, C2, and C6 carbons split into two lines: the upfield lines of C1 and C6 carbons and the downfield line of the C2 carbon are here simply assigned to the noncrystalline component, whereas the counterpart lines of these carbons are ascribed to the crystalline component. This assignment is based on the great difference in T_{1C} between the respective two lines, as shown below. More detailed assignment will be made after the line shape analysis of the spectrum. The crystalline and noncrystalline components are not resolved into the respective lines for the other carbons.

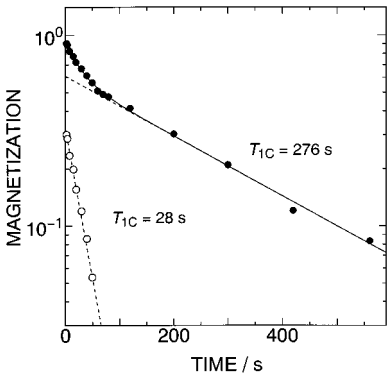

Figure 3. Semilogarithmic plots of the peak intensity of the resonance line of the crystalline component of the C6 carbon as a function of time for the relaxation, measured by the CPT1 pulse sequence. The solid line is the composite decay curve for the two components obtained by the least squares fitting, and the broken lines are the decay curves for individual components.

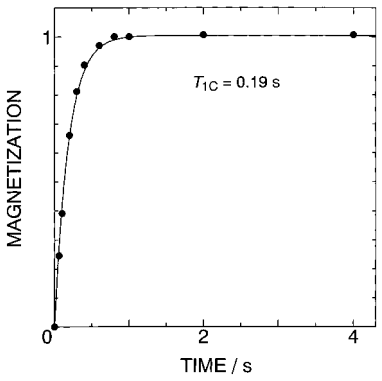

Figure 4. Plot of the peak intensity of the resonance line of the noncrystalline component of the C6 carbon as a function of time for the relaxation, measured by the saturation recovery pulse sequence. The solid line is the recovery curve obtained by the least squares fitting.

^{13}C Spin−Lattice Relaxation Analyses. Figure 3 shows the semilogarithmic spin−lattice relaxation decay curve for the peak intensity of the crystalline line of the C6 carbon, measured by the CPT1 pulse sequence.[20] Since the observed decay curve, indicated by closed circles, cannot be described by a single exponential, the least squares fitting analysis has been carried out by assuming two components with different T_{1C} values. The overall composite decay curve and the decays of the respective components are shown as solid and broken lines, respectively. The composite curve thus obtained is in good accord with the observed data, confirming the existence of two components with T_{1C} values of 276 and 28 s. Both of the two components with different T_{1C} values are assigned to the crystalline component, because these components have the same chemical shifts and therefore adopt the same conformation. This assignment is also supported by the fact that the degree of crystallinity determined by the line shape analysis based on this assignment is in good accord with the value obtained by DSC, as shown below. In contrast, the noncrystalline line of the C6 carbon has a single T_{1C} of 0.19 s, as shown in Figure 4. Here, the saturation recovery process of the magnetization of the noncrystalline line is successfully analyzed by assuming a single component.

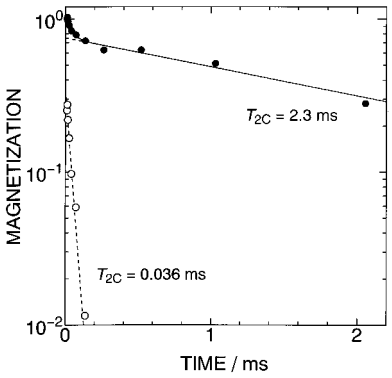

Figure 5. Semilogarithmic plots of the peak intensity of the resonance line of the noncrystalline component of the C6 carbon as a function of time for the relaxation, measured by the spin echo pulse sequence. The solid line is the composite decay curve for the two components obtained by the least squares fitting, and broken lines are the decay curves for individual components.

Table 1. T_{1C} Values for Each Carbon of PCL

	T_{1C}/s				
	C1	C2	C3, C4	C5	C6
crystalline	310	279	255, 232	232	276
	34	33	25, 27	30	28
noncrystalline	2.5	0.22	0.26, 0.26	0.21	0.19

Table 2. T_{2C} Values for the Noncrystalline Components of Each Carbon of PCL

	T_{2C}/ms				
	C1	C2	C3, C4	C5	C6
amorphous		2.5	2.6, 2.6	2.6	2.3
interfacial		0.044	0.031, 0.034	0.034	0.036

T_{1C} values thus obtained for all the carbons of PCL are summarized in Table 1. The noncrystalline component gives a single T_{1C} value, while the crystalline component has two T_{1C}. The origin of the two T_{1C}'s in the crystalline component is not clear at present, but the longer and shorter T_{1C} components possibly correspond to the rigid and mobile crystalline regions, respectively. As for the longer T_{1C} component in the crystalline region, the values of the methylene carbons become slightly shorter with increasing distance from the ester group. T_{1C} values of the crystalline component become shorter with increasing mobility under this condition. In the crystalline region, therefore, the molecular mobility with about 10^8 Hz is higher around the central part of the methylene sequence compared to that around the ester group.

^{13}C Spin−Spin Relaxation Analysis. Figure 5 shows a semilogarithmic plot of the peak intensity of the C6 carbon as a function of the time τ_t for the ^{13}C spin−spin relaxation, measured by the spin echo pulse sequence for solid-state measurements without ^{1}H dipolar decoupling during the time τ_t.[6,10] The observed decay curve, indicated by closed circles, can be clearly resolved into two parts, a rapid decay and a subsequent slow decay. T_{2C} values estimated for C2−C6 carbons of PCL by the least squares fitting are summarized in Table 2. The noncrystalline region is found to consist of two components with different T_{2C} values. The T_{2C} values of the C1 carbon are not included in this table because the data are scattered, and the T_{2C} values cannot be estimated for the C1 carbon.

Two T_{2C} values with the same orders were also found for the noncrystalline components in different polyethylene[6,9] and poly(tetramethylene oxide)[10] samples. In these polymers, the components with shorter and longer T_{2C} values were assigned to crystalline−amorphous interfacial and amorphous components, respectively. Kimura et al. confirmed this assignment by the analysis of the ^{1}H spin diffusion process for uniaxially oriented polyethylenes.[8] Therefore, the components with the shorter and longer T_{2C} values can also be assigned to the interfacial and amorphous components for the present sample, respectively.

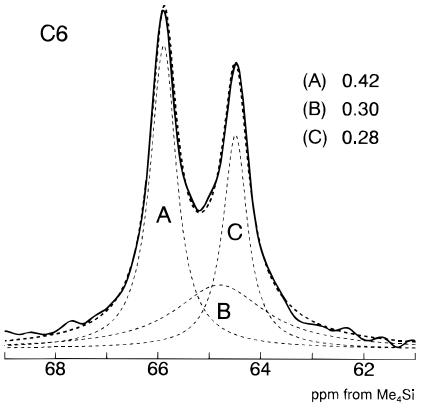

Figure 6. Component analysis of the fully relaxed ^{13}C NMR spectrum of the C6 carbon: (A) crystalline, (B) interfacial, and (C) amorphous components. The solid line is the experimental line shape and the thick broken line is the composite line shape for the three components obtained by the least squares fitting. The thin broken lines are the Lorenzians for individual components.

Line Shape Analysis. The line shape analysis of the fully relaxed, gated decoupled/MAS ^{13}C NMR spectrum shown in Figure 2 is carried out in the same manner as reported previously[6,10] to estimate the mass fraction of each component. Figure 6 shows the result of the analysis for the C6 resonance line, where the line is successfully resolved into the crystalline, interfacial, and amorphous components. Here, the respective components are assumed to be Lorentzian curves, because their line shapes separately measured are described well in terms of Lorentzians, as in the case of polyethylenes[6] and poly(tetramethylene oxide).[10] In addition, the interfacial and amorphous components can be well separated by using the difference in T_{2C} values. It should be noted here that the line widths of the interfacial and rubbery components are remarkably narrower than those expected from the T_{2C} values described above because the spectrum in Figure 6 was measured under ^{1}H dipolar decoupling. The integrated intensity fractions of the respective components thus obtained are 0.42, 0.30, and 0.28 for crystalline, interfacial, and amorphous components, respectively. The mass fraction of the crystalline component is in good accord with the degree of crystallinity (0.46) determined from the DSC measurement, where the heat of fusion for the PCL crystals was assumed to be 15.4 kJ mol^{-1}.[25] This fact also confirms the assignment of the crystalline and noncrystalline components.

2D SASS Measurement. Figure 7 shows the 2D SASS spectrum of PCL measured at room temperature. The projections along F1 and F2 axes show the conventional high-resolution spectrum and the CSA patterns for all the ^{13}C sites in PCL, respectively. The CSA in this figure is scaled by the factor $f_S = (3\cos^2\theta_S - 1)/2$ along the F1 axis by setting the isotropic resonance center as an origin. Here, $f_S = {}^1/_4$ since the spinning angle θ_S is 45°. Although CSA patterns for the C2−C5

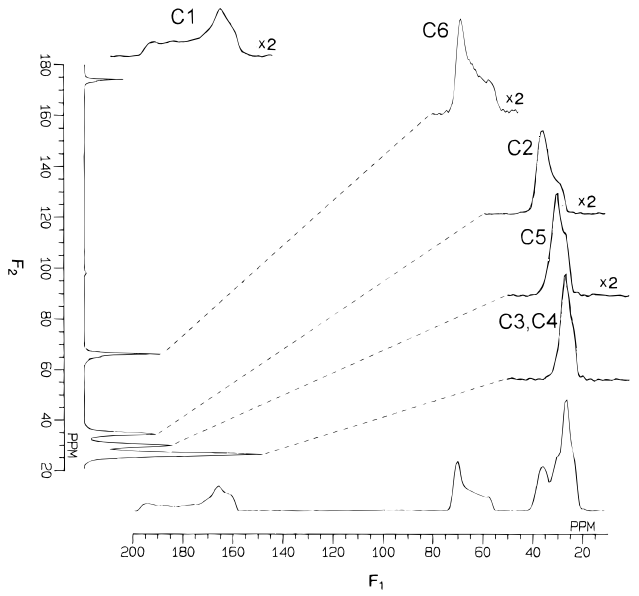

Figure 7. 2D SASS ^{13}C NMR spectrum of solid PCL. The CSA spectrum along the F_1 axis is scaled by the factor of $^1/_4$.

carbons are overlapped with each other in the projection to the F1 axis, their individual spectra are successfully recorded by taking slice spectra along the F1 axis for the isotropic resonance lines of the corresponding carbons. CSA spectra of C3 and C4 carbons cannot be still separated, because their isotropic chemical shifts are almost the same. In the 2D SASS measurement, the contribution of the noncrystalline component was negligibly small because it was obtained by using the cross polarization and the phase cycling, as shown in Figure 1. The short T_{1C} component is greatly reduced in intensity by storing the magnetization to the $+z$ and $-z$ directions alternatively during the angle switching period, which is referred to as the phase cycling here.

Figure 8 shows the descaled CSA spectra for the respective carbons of PCL, which correspond to CSA powder spectra obtained for the static sample. The CSA of the C1 carbon is almost in accord with the line shape in the rigid state.[26−29] All the other carbons exhibit the almost axially symmetric spectra, probably as a result of the motional average of the σ_{11} and σ_{22} values.

Assignment of the Principal Axes. In order to obtain the information of the molecular motion from the CSA spectra shown in Figure 8, it is necessary to carry out the assignment of the principal axes for each carbon. In this work, CP/dipole decoupled ^{13}C NMR spectra have been measured for the uniaxially oriented PCL fibers, by setting the orientation axis parallel or perpendicular to the static magnetic field B_0. Figure 9 shows the CP/dipole decoupled ^{13}C NMR spectra of the crystalline component measured by the CPT1 pulse sequence,[20] where the T_{1C} relaxation decay time was set to 8 s. Three resonance lines appear when the orientation axis is parallel to B_0. In contrast, relatively complicated resonance lines appear when the orientation axis is perpendicular to B_0.

The resonance frequency σ of a given carbon nucleus can be expressed as[30]

$$\sigma = \sigma_{11}\cos^2\alpha\sin^2\beta + \sigma_{22}\sin^2\alpha\sin^2\beta + \sigma_{33}\cos^2\beta \quad (1)$$

where α and β are the Euler angles that relate the principal axis frame for the chemical shift tensor $\boldsymbol{\sigma}$ to

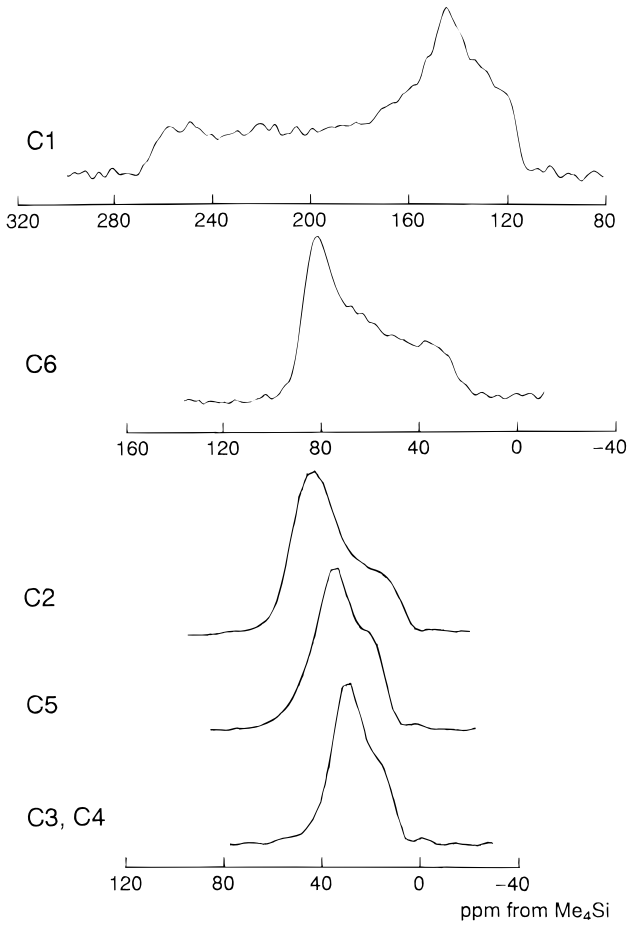

Figure 8. Descaled experimental CSA spectra for each carbon of solid PCL.

the laboratory frame. When the orientation axis is parallel to B_0, β becomes 0 for the carbon whose σ_{33} axis is parallel to the orientation axis. Then eq 1 reduces to

$$\sigma = \sigma_{33} \quad (2)$$

and thus only one resonance line is observed at σ_{33}. Similarly, eq 1 reduces to

$$\sigma = \sigma_{11} \quad (3)$$

for the carbon whose σ_{11} axis is parallel to the orientation axis. When the orientation axis is perpendicular to B_0, β becomes $\pi/2$ for the carbon whose σ_{33} axis is parallel to the orientation axis. In this case, the resonance lines are observed at σ_{11} and σ_{22} as a doublet with an equal intensity, because eq 1 reduces to

$$\sigma = \sigma_{11}\cos^2\alpha + \sigma_{22}\sin^2\alpha \quad (4)$$

Similarly, for the carbon whose σ_{11} axis is parallel to the orientation axis, eq 1 reduces to

$$\sigma = \sigma_{22}\cos^2\beta + \sigma_{33}\sin^2\beta \quad (5)$$

On the basis of these theoretical considerations, the principal axis for each carbon can be assigned from the experimental results shown in Figure 9 as follows. The values of σ_{11}, σ_{22}, and σ_{33} are shown in Figure 9 by arrows, which are obtained from the CSA spectra in Figure 8. For the methylene carbons, the averaged values, $(\sigma_{11} + \sigma_{22})/2$, are shown instead of the respective

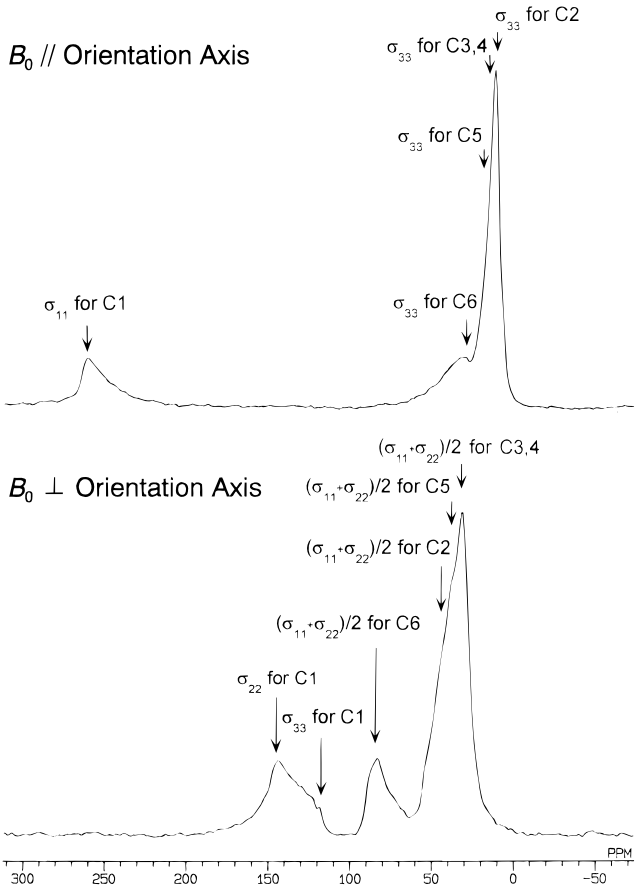

Figure 9. CP/dipole-decoupled ^{13}C NMR spectra of uniaxially oriented PCL fibers.

values, because these carbons show the axially symmetric CSA spectra at room temperature, as shown in Figure 8. According to eqs 3 and 5, we conclude that the σ_{11} axis is parallel to the orientation axis for the C1 carbon; the resonance line for this carbon is observed at σ_{11} when the orientation axis is parallel to B_0. When the orientation axis is perpendicular to B_0, the corresponding lines appear at σ_{22} and σ_{33}. The experimental line shapes are somewhat deviated from the theoretical prediction in eqs 3 and 5, possibly due to the imperfect orientation[31] or molecular motion. For the methylene carbons, the experimental line shapes in Figure 9 are also deviated from the theoretical prediction, possibly due to the molecular motion. However, the σ_{33} axis is found to be parallel to the orientation axis for all the methylene carbons from Figure 9; the resonance lines are observed at σ_{33} when the orientation axis is parallel to B_0. When the orientation axis is perpendicular to B_0, these carbons resonate not at σ_{11} and σ_{22} but at $(\sigma_{11} + \sigma_{22})/2$. This result is consistent with that for the isothermally crystallized PCL in Figure 8. Our assignments of the principal axes are in good accord with those previously reported, for example, for the methylene carbon of polyethylenes[32,33] and the carbonyl carbon of poly(methyl methacrylate).[34−36]

Simulation of CSA Spectra by the Two-Site Exchange Model. The principal values in the rigid state are necessary for the detailed analysis of the molecular motion, but they have not yet been determined for each carbon of PCL. As far as we know, however, the principal values reported for similar compounds with ester groups are not so different from those for the C1 carbon of PCL.[26−29] Therefore, the principal values obtained in this paper, $\sigma_{11} = 265$ ppm, $\sigma_{22} = 146$ ppm, and $\sigma_{33} = 117$ ppm, will be used for the CSA simulation of the C1 carbon described below. In contrast, the principal values of the methylene carbon directly attached to the oxygen atom seem to depend on the type of compound.[37−41] In the present analysis, $\sigma_{11} = 106$ ppm, $\sigma_{22} = 91$ ppm, and $\sigma_{33} = 27$ ppm[37] for the OCH_2 carbon of poly(tetramethylene oxide), which are determined at −90 °C, are assumed as the principal values for the C6 carbon in the rigid state. As for the principal values of the C3−C5 carbons, $\sigma_{11} = 52$ ppm, $\sigma_{22} = 37$ ppm, and $\sigma_{33} = 13$ ppm, which are derived from the values determined for polyethylenes crystals,[33,42,43] are used as reference values in the rigid state. The principal values are not assumed for the C2 carbon in this work.

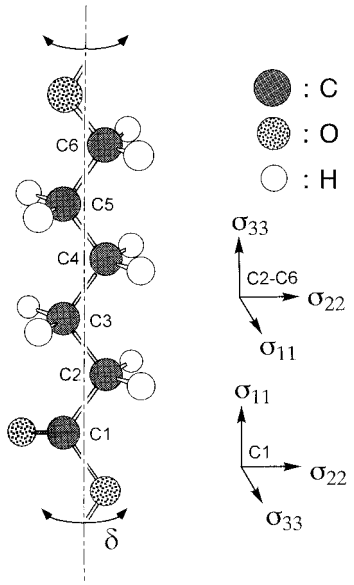

Figure 10. Schematic model of the jump motion around the molecular chain axis for PCL in the crystalline state.

Based on the principal axes and their values determined above, the simulation of CSA spectra is carried out by using the two-site exchange model.[44,45] In this case, each carbon of PCL is assumed to undergo a jump motion around the molecular chain axis with a jump angle δ and a jump rate κ between two sites. The analysis by the two-site exchange model is possibly based on the existence of the conformational distortion of the methylene chain from the planar zigzag conformation, as shown below. Figure 10 shows the schematic model of the jump motion around the molecular chain axis of PCL in the crystalline state, where the principal axes are also shown for the carbonyl and methylene carbons.

Figure 11 shows the simulated CSA spectra for the C1 carbon with different jump angles and jump rates. The wiggles on the simulation spectra in Figure 11b−g (and Figures 12g and 13g, as shown below) are numerical noise. The slow and fast exchange limits of the jump motion are about 10^2 and 10^4 Hz, respectively. When the jump angle is less than 30°, the line shape is almost the same as that in the rigid state at any jump rate. When the jump angle is larger than 30°, significant narrowing due to the average of σ_{22} and σ_{33} is observed for the higher jump rates. In the present case, the exact jump angle and frequency cannot be determined because the principal values in the rigid state are not well-defined at present. Nevertheless, the experimental line shape of the C1 carbon is definitely different from the simulated line shape for the jump

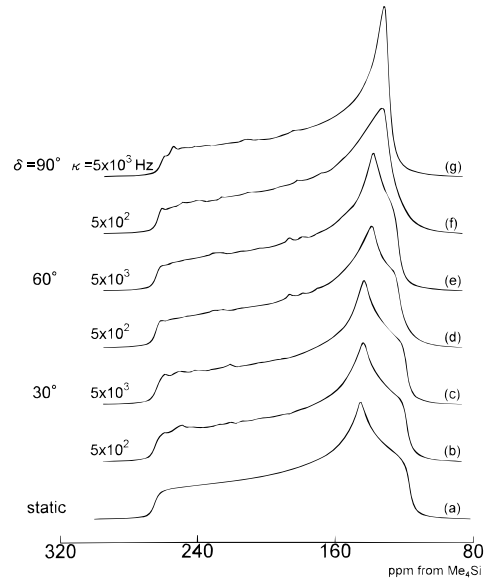

Figure 11. Simulated CSA spectra for the C1 carbon of PCL.

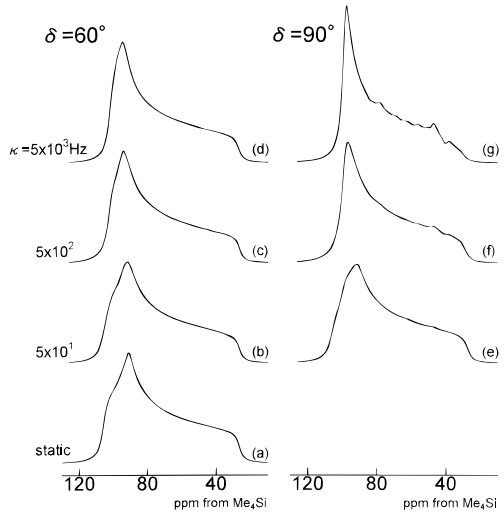

Figure 12. Simulated CSA spectra for the C6 carbon of PCL.

motion with $\delta > 30°$. Therefore, the C1 carbon is concluded to be static or to undergo the jump motion with $\delta < 30°$.

Figure 12 shows the simulated CSA spectra for the C6 carbon with different jump rates for $\delta = 60°$ and 90°. Similar to the case of the C1 carbon, the line shape is almost the same as that in the rigid state at any jump rate, when the jump angle is less than 30° (not shown here). The simulated CSA spectra are wider than the experimental ones. Since the reported principal values of the OCH_2 carbons depend on compounds,[37−41] only the shapes of CSA spectra should be discussed here. The comparison between the simulated and experimental CSA spectra suggests that the C6 carbon undergoes 60−90° jump motion around the chain axis with the frequency of about 10^2−10^3 Hz. Although the simulation has not been carried out for the C2 carbon, the axially symmetric CSA line shape indicates that this carbon also seems to undergo the same type of 60−90° jump motion.

Figure 13 shows the simulated CSA spectra for the C3−C5 carbons, which are obtained by assuming the same type of jump motion around the chain axis. Experimental spectra for the C3 and C4 carbons are narrower than the simulated spectra for the 60−90° jump motion. This may be due to the additional partial averaging of σ_{33}, suggesting an additional molecular motion, probably around the C−C bond, for these carbons.

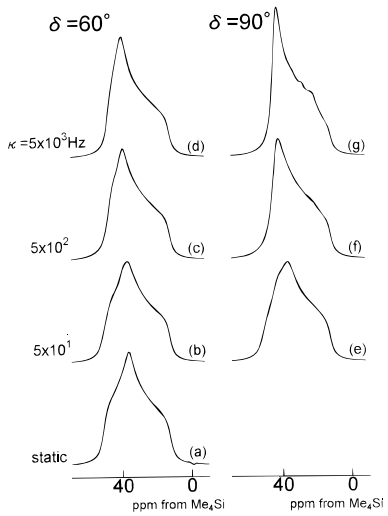

Figure 13. Simulated CSA spectra for the C3−C5 carbons of PCL.

In summary, the C1 carbon is almost rigid or undergoes the jump motion around the molecular chain axis with $\delta < 30°$. C2 and C6 carbons adjacent to the ester group undergo the 60−90° jump motion around the molecular chain axis. C3 and C4 carbons, which are not directly attached to the ester group, additionally undergo some molecular motion, probably around the C−C bond.

In this paper, the simulation of CSA line shapes has been carried out on the assumption that individual carbons undergo the two-site jump motion around the molecular chain axis. From the results of the simulation, however, it is possible for individual carbons to undergo not the cooperative jump motion around the molecular chain axis but the wavelike motion where the ester group is almost rigid and methylene carbons undergo the 60−90° jump motion around the chain axis with or without the additional molecular motion. The molecular motion accompanied by the conformational changes cannot be analyzed by the CSA line shapes, because the principal values will change depending on the conformation. In order to obtain the more detailed information of the molecular motion, the C−H dipolar spectra or ^2H spectra, which are independent of the conformational change, will be analyzed in the near future.

Similar motional inhomogeneities have been observed in several systems. English et al. analyzed the methylene motion in the crystalline component of nylon 66 in detail by solid-state ^2H NMR measurements[46] and molecular dynamics simulation.[47] The functional group of nylon 66 is almost rigid in the crystalline region, while the methylene carbons undergo the librational motion around the chain axis with $\delta \cong 60°$ above 100 °C. This temperature is almost the same as or slightly above the temperature at which the methylene carbons in polyethylenes begin to undergo the 180° jump motion around the chain axis with a frequency of 10^4−10^5 Hz.[48,49] Compared with these polymers with fully extended methylene chains, the present results indicate that the methylene chain in PCL is mobile even at 41 °C. This is probably because the methylene chain in PCL is slightly distorted. Two types of conformations

are reported for PCL by the X-ray diffraction measurements: one is the planar zigzag conformation,[2] and the other is a slightly distorted nonplanar zigzag conformation.[3] A recent electron diffraction study revealed that the latter conformation is more suitable.[4] If such a conformational distortion really exists, the potential energy curve of methylene carbons in PCL will not be single but double-welled. In this case, the jump motion may be induced between the two potential wells, suggesting the enhanced molecular mobility for methylene sequences in PCL compared to the fully extended methylene sequences in polyethylenes. This sort of crystalline state of PCL may correspond to one of dynamic conformational disordered states.[50−52]

Ultraslow motions in PCL were also investigated by two-dimensional ^{13}C CSA exchange measurements. Two-dimensional CSA exchange spectra for C1 and C6 carbons, which were separately observed by using off magic angle spinning with the angle of 45°, do not show observable off-diagonal peaks with mixing times between 0.1 and 3 s, indicating that ultraslow motions with a frequency of 10^{-1}−10^{1} Hz are almost frozen for C1 and C6 carbons.

Conclusion

One- and two-dimensional ^{13}C NMR analyses of the crystalline−noncrystalline structure and molecular motion in the crystalline region have been performed at room temperature for poly(ϵ-caprolactone) (PCL) isothermally crystallized from the melt at 50 °C for 4 days.

(1) ^{13}C spin−lattice relaxation time (T_{1C}) and ^{13}C spin−spin relaxation time (T_{2C}) analyses have been carried out to characterize the crystalline−noncrystalline structure. T_{1C} analyses have revealed that three components exist with different T_{1C} values, which are assignable to the crystalline, mobile crystalline, and noncrystalline components. T_{2C} analyses have also revealed that in the noncrystalline region, two components exist with different T_{2C} values, which are assignable to crystalline−amorphous interfacial and amorphous components.

(2) From the line shape analysis of the fully relaxed, gated decoupled/MAS ^{13}C NMR spectrum of PCL, the mass fractions of the crystalline, crystalline−amorphous interfacial, and amorphous components are determined to be 0.42, 0.30, and 0.28, respectively. The mass fraction of the crystalline component is in good accord with the degree of crystallinity as determined by DSC measurement.

(3) T_{1C} values of the respective carbons in the crystalline component become slightly shorter with increasing distance from the ester group, suggesting that the methylene carbons undergo more enhanced molecular motion with the increase of the distance from the ester group, even in the crystalline state.

(4) More detailed molecular motion with the order of 10^3 Hz in the crystalline region has been characterized by analyzing the ^{13}C chemical shift anisotropy (CSA) in terms of the two-site exchange model. ^{13}C CSA spectra of the individual carbons of PCL can be successfully recorded by using the two-dimensional switching angle sample spinning method. The CSA spectrum for the carbonyl carbon thus obtained almost agrees with that in the rigid state. In contrast, methylene carbons exhibit axially symmetric CSA spectra, suggesting rapid jump motions around the molecular chain axis with jump angles of 60−90°. In particular, much narrower CSA spectra with axial symmetry are observed for the methylene carbons in the central part of the sequence, suggesting the existence of additional enhanced jump motion around the C−C bonds. Such enhanced methylene motions may be related to the conformational distortion from the planar zigzag conformation.

Acknowledgment. The poly(ϵ-caprolactone) pellets and fibers were kindly supplied by Mr. Tsuyoshi Murata of Unitika Co. Ltd. Computation time was provided by the Supercomputer Laboratory, Institute for Chemical Research, Kyoto University. Financial support from a Grant-in-Aid for Encouragement of Young Scientists (07750993), from the Ministry of Education, Science, and Culture, Japan, is gratefully acknowledged.

References and Notes

(1) Goulet, L.; Prud'homme, R. E. *J. Polym. Sci., Part B* **1990**, *28*, 2329.
(2) Bittiger, H.; Marchessault, R. H. *Acta Crystallogr.* **1970**, *B26*, 1923.
(3) Chatani, Y.; Okita, Y.; Tadokoro, H.; Yamashita, Y. *Polym. J.* **1970**, *1*, 555.
(4) Hu, H.; Dorset, D. L. *Macromolecules* **1990**, *23*, 4604.
(5) For example: Komorski, R. A. *High Resolution NMR Spectroscopy of Synthetic Polymers in Bulk*; VCH: Dearfield Beach, 1986.
(6) Kitamaru, R.; Horii, F.; Murayama, K. *Macromolecules* **1986**, *19*, 636.
(7) Saito, S.; Moteki, T.; Nakagawa, M.; Horii, F.; Kitamaru, R. *Macromolecules* **1990**, *23*, 3257.
(8) Kimura, T.; Neki, K.; Tamura, N.; Horii, F.; Nakagawa, M.; Odani, H. *Polymer* **1992**, *33*, 493.
(9) Kiramaru, R.; Horii, F.; Zhu, Q.; Bassett, D. C.; Olley, R. H. *Polymer* **1994**, *35*, 1171.
(10) Hirai, A.; Horii, F.; Kitamaru, R.; Fatou, J. G.; Bello, A. *Macromolecules* **1990**, *23*, 2913.
(11) Tsuji, H.; Horii, F.; Nakagawa, M.; Ikada, Y.; Odani, H.; Kitamaru, R. *Macromolecules* **1992**, *25*, 4114.
(12) Horii, F.; Hu, S.; Ito, T.; Odani, H.; Matsuzawa, S.; Yamaura, K. *Polymer* **1992**, *33*, 2299.
(13) Hu, S.; Tsuji, M.; Horii, F. *Polymer* **1994**, *35*, 2516.
(14) Ishida, M.; Yoshinaga, K.; Horii, F. *Macromolecules* **1997**, *29*, 8824.
(15) Yamamoto, H.; Horii, F. *Macromolecules* **1993**, *26*, 1313.
(16) Yamamoto, H.; Horii, F. *Cellulose* **1994**, *1*, 57.
(17) Mathias, L. J. *Solid State NMR of Polymers*; Plenum Press: New York, 1991.
(18) Schmidt-Rohr, K; Spiess, H. W. *Multidimensional Solid-State NMR and Polymers*; Academic Press: New York, 1994.
(19) Kaplan, M. L.; Bovey, F. A.; Chang, H. V. *Anal. Chem.* **1975**, *47*, 1703.
(20) Torchia, D. A. *J. Magn. Reson.* **1978**, *30*, 613.
(21) Bax, A.; Szeverenyi, N. M.; Maciel, G. E. *J. Magn. Reson.* **1983**, *55*, 494.
(22) Terao, T.; Fujii, T.; Onodera, T.; Saika, A. *Chem. Phys. Lett.* **1984**, *107*, 147.
(23) Horii, F.; Beppu, T.; Takaesu, N.; Ishida, M. *Magn. Reson. Chem.* **1994**, *32*, S30.
(24) Kricheldorf, H. R.; Berl, M.; Scharnagl, N. *Macromolecules* **1988**, *21*, 286.
(25) Crescenzi, V.; Manzini, G.; Calzolari, G.; Borri, C. *Eur. Polym. J.* **1972**, *8*, 449.
(26) Cornell, B. A. *Chem. Phys. Lett.* **1980**, *72*, 462.
(27) Linder, M.; Hohener, A.; Ernst, R. R. *J. Chem. Phys.* **1980**, *73*, 4959.
(28) Pines, A.; Gibby, M. G.; Waugh, J. S. *Chem. Phys. Lett.* **1972**, *15*, 373.
(29) Edzes, H. T. *Polymer* **1983**, *24*, 1425.
(30) Mehring, M. *Principles of High Resolution NMR in Solids*, 2nd ed.; Springer: Berlin, 1983.
(31) Asakura, T.; Konakazawa, T.; Demura, M.; Ito, T.; Maruhashi, Y. *Polymer* **1996**, *37*, 1965.
(32) VanderHart, D. L. *J. Chem. Phys.* **1976**, *64*, 830.
(33) Nakai, T.; Ashida, J.; Terao, T. *J. Chem. Phys.* **1988**, *88*, 6049.
(34) Kulik, A. S.; Spiess, H. W. *Makromol. Chem.* **1994**, *195*, 1755.
(35) Schmidt-Rohr, K.; Kulik, A. S.; Beckham, H. W.; Ohlemacher, A.; Pawelzik, U.; Boeffel, C.; Spiess, H. W. *Macromolecules* **1994**, *27*, 4733.

(36) Dabbagh, G.; Weliky, D. P.; Tycko, R. *Macromolecules* **1994**, *27*, 6183.
(37) Kaji, H.; Kuwabara, K.; Horii, F. *Polym. Prepr., Jpn.* **1995**, *44*, 2917.
(38) Fleming, W. W.; Fyfe, C. A.; Kendrick, R. D.; Lyerla, J. R.; Vanni, H.; Yannoni, C. S. In *Polymer Characterization by ESR and NMR*; Woodward, A. E., Bovey, F. A., Eds.; ACS Symposium Series 142; American Chemical Society: Washington, DC, 1980; p 193.
(39) Murphy, P. B.; Taki, T.; Gerstein, B. C.; Henrichs, P. M.; Massa, D. J. *J. Magn. Reson.* **1982**, *49*, 99.
(40) Pines, A.; Gibby, M. G.; Waugh, J. S. *Chem. Phys. Lett.* **1972**, *15*, 373.
(41) Hohener, A. *Chem. Phys. Lett.* **1978**, *53*, 97.
(42) Urbina, J.; Waugh, J. S. *Proc. Natl. Acad. Sci.* **1974**, *71*, 5062.
(43) VanderHart, D. L. *Macromolecules* **1979**, *12*, 1232.
(44) Abragam, A. *The Principles of Nuclear Magnetism*; Clarendon Press: Oxford, U.K., 1989; p 450.
(45) Horii, F.; Uyeda, T.; Beppu, T.; Murata, T.; Odani, H. *Bull. Inst. Chem. Res. Kyoto Univ.* **1992**, *70*, 198.
(46) Hirschinger, J.; Miura, H.; Gardner, K. H.; English, A. D. *Macromolecules* **1990**, *23*, 2153.
(47) Wendoloski, J. J.; Gardner, K. H.; Hirschinger, J.; Miura, H.; English, A. D. *Science* **1990**, *247*, 431.
(48) Horii, F.; Kitamaru, R. *J. Polym. Sci., Polym. Phys. Ed.* **1981**, *19*, 109.
(49) Kuwabara, K.; Kaji, H.; Horii, F.; Bassett, D. C.; Olley, R. H. *Polym. Prepr., Jpn.* **1996**, *45*, 3259.
(50) Wunderlich, B.; Moller, M.; Grebowicz, J.; Baur, H. *Conformational Motion and Disorder in Low and High Molecular Mass Crystals*; Advances in Polymer Science; Springer Verlag: Berlin, 1988; Vol. 87.
(51) Wunderlich, B.; Grebowicz, J. In *Liquid Crystalline Polymers II/III*; Gordon, M., Plate, N. A., Eds.; Advances in Polymer Science; Springer Verlag: Berlin, 1984; Vols. 60/61, p 1.
(52) Xenopoulos, A.; Cheng, J.; Yasuniwa, M.; Wunderlich, B. *Mol. Cryst. Liq. Cryst.* **1992**, *214*, 63.

MA970167L